

Beam Growth Measurements in RHIC with Gold at Injection

W. Fischer, M. Bai, J.M. Brennan, M. Blaskiewicz, P. Cameron,
R. Connolly, A. Lehrach, G. Parzen, S. Tepikian, J. v. Zeijts and K. Zeno

March 20, 2000

Abstract

To fill the RHIC rings, bunches are stored for up to several minutes at the injection energy before acceleration starts. A bunch length increase during this time may lead to particle loss during transition crossing and rebucketing into storage buckets. Transverse beam growth during this time will ultimately decrease the attainable luminosity. The measurement, understanding and possible limitation of beam growth at injection is therefore desirable. Measurements of longitudinal and transverse growth are presented for gold beams. Comparisons with computations of intrabeam growth times are shown.

1 Introduction

Several minutes are needed to fill both RHIC rings. Some bunches are stored for this entire time at the injection energy before acceleration starts. During this time the beam can grow both longitudinally and transversely.

An increase in bunch length, and a corresponding increase in the longitudinal emittance, may be induced by rf noise or intrabeam scattering. The latter is particularly severe for high-charge particles like fully stripped gold ions. Earlier computations yielded longitudinal beam growth rates from intrabeam scattering of a few minutes [1, 2]. An increase in the longitudinal emittance may lead to particle loss during transition. Particles with large momentum deviations also experience stronger tune modulation in case of non-zero chromaticities. Tune modulation in conjunction with nonlinear magnetic fields can limit the beam life time [3]. Furthermore, when bunches become too long they cannot be transferred into the buckets of the storage rf system.

Effects that can contribute to transverse beam growth include nonlinear magnetic fields, tune ripple, rest gas scattering, and space charge. Transverse emittance growth reduces the luminosity that can be achieved with the fill.

In the following we present beam growth observations for gold beam at injection made during the RHIC Run 2000. For this run a lattice was used with $\beta^* = 8$ m at the 6 o'clock and 10 o'clock interaction points and $\beta^* = 3$ m at all other interaction points. Basic machine parameters are given in Tab. 1. In Sec. 2 a short description of all used measurement devices is given and measurement results are shown. In Sec. 3 an analysis of the measured data is presented.

Table 1: RHIC Machine parameters for gold operation in 2000, at injection.

Parameter	Symbol	Unit	Value
Relativistic gamma	γ	1	10.25
Transition gamma	γ_{tr}	1	22.8
Slip factor	η	1	-0.00759
Rf voltage per turn	V_{rf}	kV	300
Harmonic number	h	1	360
Revolution frequency	f_{rev}	kHz	77.82
Synchrotron frequency	f_s	Hz	185
Bucket length	l	ns	35.69

2 Measurements

A total of 12 dedicated beam growth measurements were recorded on four different days. In all cases a single bunch of gold ions was injected into the Blue ring, and observed over several minutes. These measurements are summarized in Tab. 2. The pre-accelerators were carefully tuned in order to obtain a high bunch intensity in RHIC. The closed orbit in the ring was corrected. To minimize transverse emittance blow-up caused by the injection mis-steering, the injection was optimized. Ring closed orbits were saved as well as the first 128 turns of the injected beam. From the latter the transverse tunes were determined as well as an estimate for the coupling in the machine. Tab. 3 shows the recorded machine conditions for the measured cases. The following quantities were recorded for a beam growth measurement:

1. the total intensity with a beam current transformer (BCT)
2. the bunched intensity with a wall current monitor (WCM)
3. the longitudinal profile with a wall current monitor (WCM)
4. the transverse beam sizes with the ionization profile monitor (IPM)
5. the longitudinal Schottky spectrum with a Schottky detector

The recording devices are briefly described below. The data for all cases recorded are presented for each device.

2.1 Beam Current Transformer

The RHIC beam current transformers have two gain settings to cover a wide intensity range. In the high gain mode a maximum beam current of 5 mA ($5 \cdot 10^9$ gold ions) can be measured, in the low gain mode up to 500 mA ($500 \cdot 10^9$ gold ions). For the beam growth measurements, the beam current monitor was used in the low gain mode since a single bunch with approximately $0.5 \cdot 10^9$ gold ions (0.5 mA) was observed.

Table 2: Overview of beam growth measurements at injection energy.

case no	time	intensity			lifetime		rms length	hor rms size [mm]	ver rms size [mm]	bunch area 95% [eV·s/u]	hor norm. emitt. [μm]	ver norm. emitt. [μm]	space charge ξ_{max} [10 ¹²]	measured growth time			
		total [10 ⁶]	bunched [10 ⁶]	beam [%]	total [min]	bunched [min]								length [min]	hor [min]	ver [min]	
initial																	
1	04:56	430	430	100	7	19	4.34	—	—	0.51	—	—	24.2	-0.009	53	—	—
2	18:52	589	571	97	55	89	5.31	—	—	0.77	—	—	27.1	-0.010	183	—	—
3	19:15	711	710	100	37	19	5.43	—	—	0.80	—	—	31.9	-0.011	208	—	—
4	10:34	242	208	86	8	39	6.33	—	—	1.09	—	—	9.3	-0.003	-57	—	—
5	10:53	216	212	98	4	3	5.97	—	—	0.97	—	—	8.8	-0.003	-11	—	—
6	10:55	229	223	97	74	64	5.36	—	—	0.78	—	—	10.4	-0.004	-172	—	—
7	11:06	261	243	93	84	36	6.33	—	6.3	1.09	—	13.8	10.0	-0.004	-58	—	—
8	11:24	424	416	98	34	46	5.60	—	6.1	0.85	—	13.2	18.5	-0.007	-74	—	—
9	11:51	565	518	92	10	58	5.48	9.3	6.2	0.82	30.4	13.6	25.1	-0.009	-122	20	78
10	12:18	486	422	87	13	23	7.37	9.0	5.8	1.48	28.8	11.8	16.1	-0.006	-30	26	52
11	12:17	505	505	100	17	42	4.55	—	6.2	0.56	—	13.6	27.0	-0.010	110	—	—
12	12:42	451	451	100	11	56	4.64	—	—	0.59	—	—	23.7	-0.008	165	—	—
final																	
1	05:09	397	397	100	859	153	5.07	—	—	0.70	—	—	19.1	-0.007	179	—	—
2	19:05	536	485	90	232	96	5.52	—	—	0.83	—	—	23.7	-0.008	361	—	—
3	19:27	629	548	87	216	37	5.51	—	—	0.83	—	—	27.8	-0.010	273	—	—
4	10:54	216	175	81	276	99	5.54	—	—	0.83	—	—	9.5	-0.003	-129	—	—
5	10:56	200	192	96	10	13	5.75	—	—	0.90	—	—	8.5	-0.003	-39	—	—
6	11:04	223	209	94	1271	143	5.19	—	—	0.73	—	—	10.5	-0.004	-8975	—	—
7	11:23	251	205	82	803	87	5.53	—	7.0	0.83	—	17.2	11.0	-0.004	-246	—	—
8	11:50	398	322	81	984	110	5.19	—	6.4	0.73	—	14.6	18.7	-0.007	-3857	—	—
9	12:18	505	390	77	282	100	5.21	17.9	8.0	0.74	113.9	22.8	23.6	-0.008	-926	46	188
10	12:46	417	284	68	169	57	5.09	11.4	7.6	0.70	46.2	20.3	20.0	-0.007	-199	385	219
11	12:42	433	378	87	231	67	5.09	—	6.8	0.70	—	20.7	20.0	-0.007	464	—	—
12	13:06	386	343	89	8669	106	5.04	—	—	0.69	—	—	18.7	-0.007	361	—	—
change initial – final (except time [min] all other numbers are given in [%])																	
1	13.3	-8	-8	0	11962	725	17	—	—	37	—	—	-21	-21	236	—	—
2	13.3	-9	-15	-7	324	8	4	—	—	8	—	—	-12	-12	97	—	—
3	12.6	-12	-23	-13	491	93	1	—	—	3	—	—	-13	-13	31	—	—
4	20.3	-11	-16	-6	3340	152	-12	—	—	-23	—	—	2	2	124	—	—
5	1.7	-7	-9	-2	162	339	-4	—	—	-7	—	—	-4	-4	253	—	—
6	9.2	-3	-6	-4	1608	130	-3	—	—	-6	—	—	0	0	5124	—	—
7	17.3	-4	-16	-12	858	146	-13	—	11	-24	—	24	10	10	326	—	—
8	26.1	-6	-22	-17	2812	137	-7	—	5	-14	—	11	1	1	4721	—	—
9	26.5	-11	-25	-16	2831	74	-5	94	29	-10	274	67	-6	-6	661	129	140
10	28.3	-14	-33	-22	1218	148	-31	27	31	-52	60	72	24	24	561	1361	325
11	24.7	-14	-25	-13	1299	59	12	—	10	25	—	21	-23	-23	161	—	—
12	24.3	-14	-24	-11	76362	91	8	—	—	18	—	—	-21	-21	119	—	—

Table 3: Machine conditions for the measured cases. Empty fields denote missing experimental data.

case no	date	WCM used	closed orbit				tunes			trans. coupl. beat period [turns]
			horizontal rms [mm]	horizontal max [mm]	vertical rms [mm]	vertical max [mm]	synchr. [1]	hor. [1]	ver. [1]	
1	08/11/00	WCM4	–	–	–	–	0.0024	–	–	yes –
2	08/14/00	WCM4	–	–	–	–	0.0024	0.222	0.229	yes –
3	08/14/00	WCM4	–	–	–	–	0.0024	0.222	0.229	yes –
4	08/30/00	WCM2	1.2	3.9	1.3	6.8	0.0024	0.236	0.230	yes 100
5	08/30/00	WCM2	1.2	3.9	1.3	6.8	0.0024	0.237	0.230	yes 100
6	08/30/00	WCM2	1.2	3.9	1.3	6.8	0.0024	0.237	0.230	yes 100
7	08/30/00	WCM2	1.2	3.9	1.3	6.8	0.0024	0.238	0.230	yes 100
8	08/30/00	WCM2	1.2	3.9	1.3	6.8	0.0024	0.222	0.230	yes 100
9	08/30/00	WCM2	1.2	3.9	1.3	6.8	0.0024	0.239	0.237	yes 100
10	08/30/00	WCM2	1.2	3.9	1.3	6.8	0.0024	0.238	0.228	yes 100
11	09/01/00	WCM2	2.0	9.7	1.2	3.8	0.0024	0.239	0.218	yes 70
12	09/01/00	WCM2	2.0	9.7	1.2	3.8	0.0024	0.241	0.221	yes 70

The analog signal is transformed into digital data with a 20-bit ADC. The data acquisition rate is 1 Hz. The noise level is less than 1 μA . The resolution and long term stability is better than $\pm 10 \mu\text{A}$ from dc to 100 Hz, the drift is better than $\pm 10 \mu\text{A}$ over 10 hours, the absolute accuracy is better than 0.1% at full scale, and the linearity is better than 0.1%.

In Fig. 1 the intensities of all measured cases are shown, normalized to the initial intensities. To obtain beam lifetimes from these data, a polynomial function, typically of 5th order, was fitted to the data. The lifetime can then be computed as the derivative of the fitted function. Higher order polynomials usually provide better fits but may have relatively large changes in their derivatives from which the lifetime is determined. The robustness of the lifetime estimates therefore deteriorates with the polynomial order. The used order is a compromise between the two effects. In some cases the fit could not be extended over the whole measurement range. In these cases, the first 200 s were fitted with one polynomial function, and the remaining data with a second polynomial function. Measured intensities and fitted beam lifetimes, at the beginning and at the end of a measurement, are summarized in Tab. 2.

2.2 Wall Current Monitor

Wall current monitors were used for two purposes. First, the bunched beam intensity was measured, and second, the longitudinal bunch length was determined as a function of time. Two wall current monitors were used for the measurements, one at 4 o'clock and one at 2 o'clock. The wall current monitors give the instantaneous beam current as a function of time. The resolution of both devices was 0.25 ns. A longitudinal profile was recorded every 4 s. The wall current monitor at 2 o'clock took the average of 128 turns every 4 s.

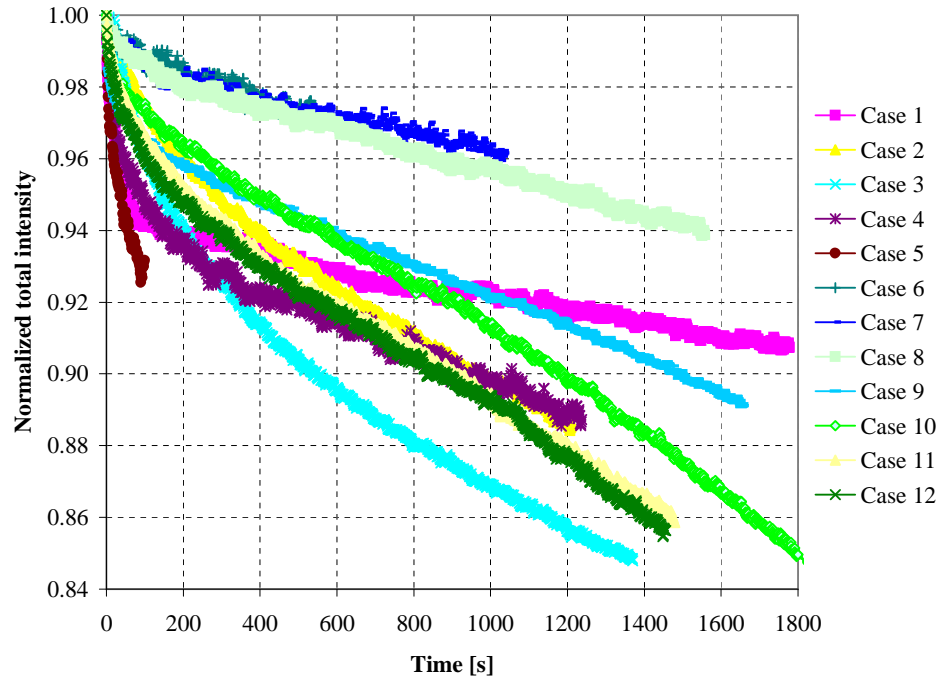
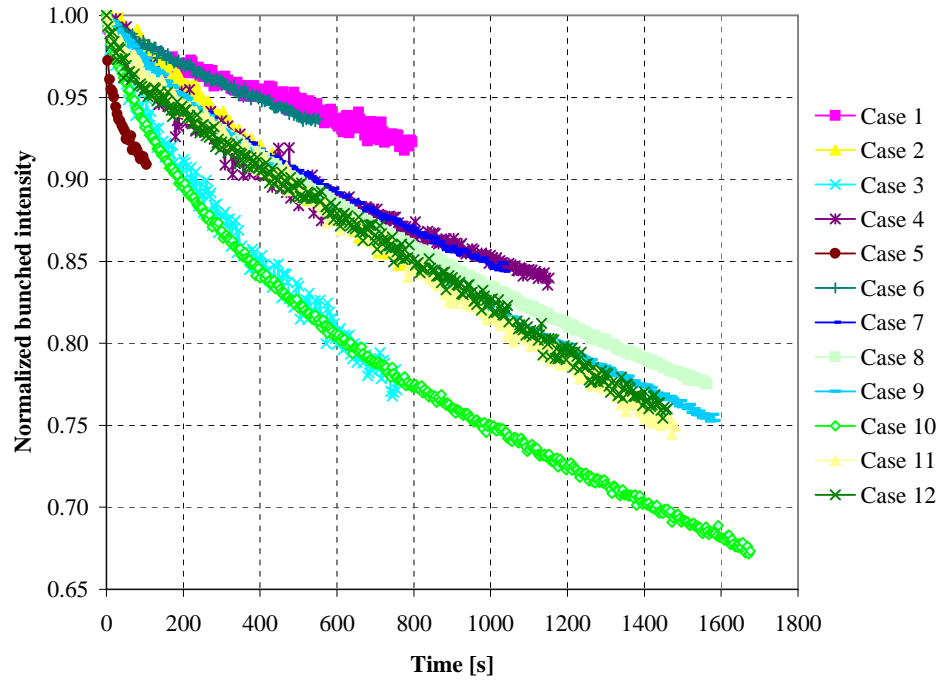


Figure 1: Total beam intensities of all measured cases, normalized to the initial intensities.



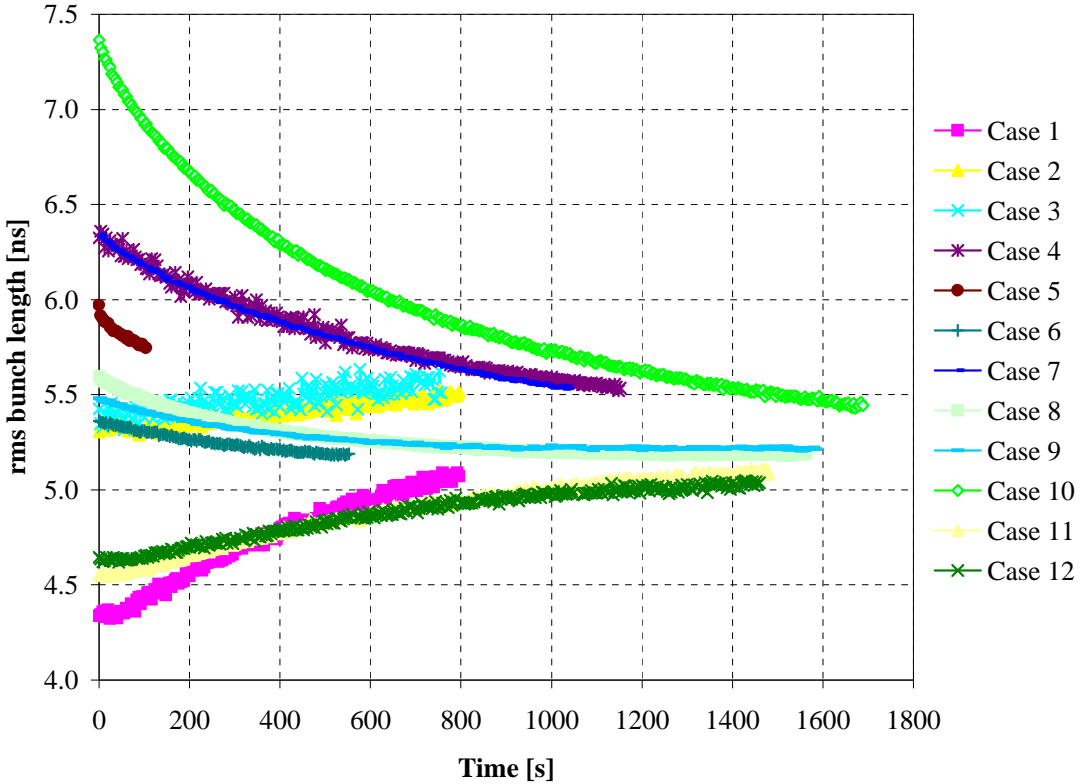


Figure 3: Bunch length evolution of all measured cases. Shown are one standard deviation of a Gaussian fit to the longitudinal profiles.

The bunched intensity was obtained as the integral under the longitudinal profile. Fig. 2 shows the measured bunched intensities for all cases, normalized to the initial intensities. The bunched beam lifetimes were determined in the same way as the total intensity lifetime. The lifetimes are given in Tab. 2.

The longitudinal profiles were fitted with a Gaussian function. Fig. 3 shows the time evolution of the fitted standard deviation for all cases. Note that initially long bunches shrink and initially short bunches grow. The bunch lengths approach values between 5 ns and 5.5 ns, with an average of 5.2 ns.

Longitudinal profiles at the beginning and end of a measurement are shown in Figs. 4 and 5. Due to a mismatched longitudinal injection, the beam was injected into the Blue ring with a sizeable momentum or phase error in measurement cases 4 through 10. This resulted in large initial bunch areas and, after filamentation, in a double peak structure in the longitudinal profile, visible in Fig. 4. At the end of a measurement the intensity is reduced from particles lost out of the bucket and the bunch length is reduced. In addition, the double peak structure is lost and the profile fits well to a Gaussian function.

In Fig. 5 a case with good longitudinal injection is show. The bunch length grows over the measurement period. In this case too, particles are lost out of the bucket.

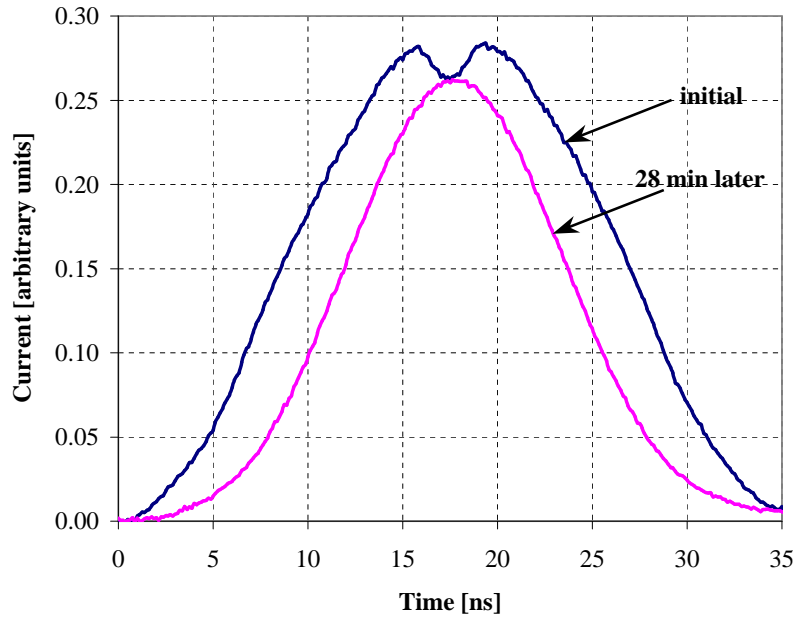


Figure 4: Longitudinal profile at the beginning and at the end of a measurement (case 10). This beam was injected with a significant phase or momentum error. The bunch length is reduced at the end of the measurement.

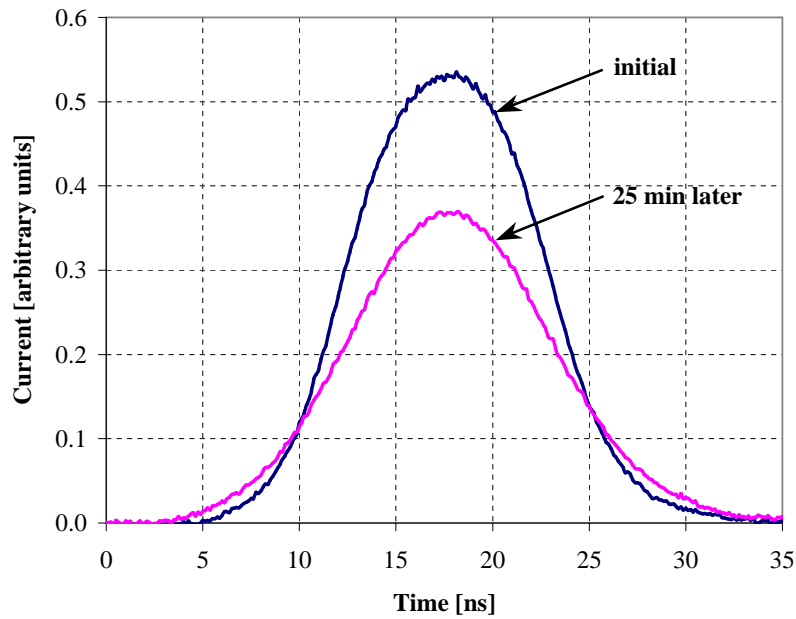


Figure 5: Longitudinal profile at the beginning and at the end of a measurement (case 11). In this case the longitudinal injection had the correct phase and momentum. The bunch length is increased at the end of the measurement.

2.3 Ionization Profile Monitor

Beam profiles were measured with the horizontal and vertical ionization beam profile monitor (IPM) in the Blue ring. An IPM measures the distribution of electrons in the beam line resulting from residual gas ionization during bunch passage. The electrons are swept transversely from the beam line and collected on 64 strip anodes oriented parallel to the beam axis. At each bunch passage the charge pulses are amplified, integrated, and digitized. The profiles shown here were produced by averaging 200 consecutive turns.

The IPM's performed well during the 1999 commissioning run and early in the 2000 run. However as the bunch intensity increased there was a beam-induced ringing that increased in amplitude until it saturated the amplifiers and made the IPM's unusable. This ringing was traced to a copper-mesh window placed over the micro channel plate input and capacitively grounded around its perimeter to prevent beam-anode coupling. When a beam bunch passed it induced a low-frequency longitudinal oscillation in the rf screen which was picked up by the anodes. Near the end of the run the vertical IPM in the Blue ring was fixed in time for the measurements reported here. Fig. 6 shows a horizontal and a vertical ionization profile from the monitor. Figures 7 and 8 show the time evolution of the measured horizontal and vertical rms beam sizes. During the first 200 s of case 8 and case 9 the charge sensitive amplifiers for center plate channels were saturated and the beam size is overstated. After amplification adjustment the correct beam size is shown. Due to the ringing problem the horizontal data are not reliable.

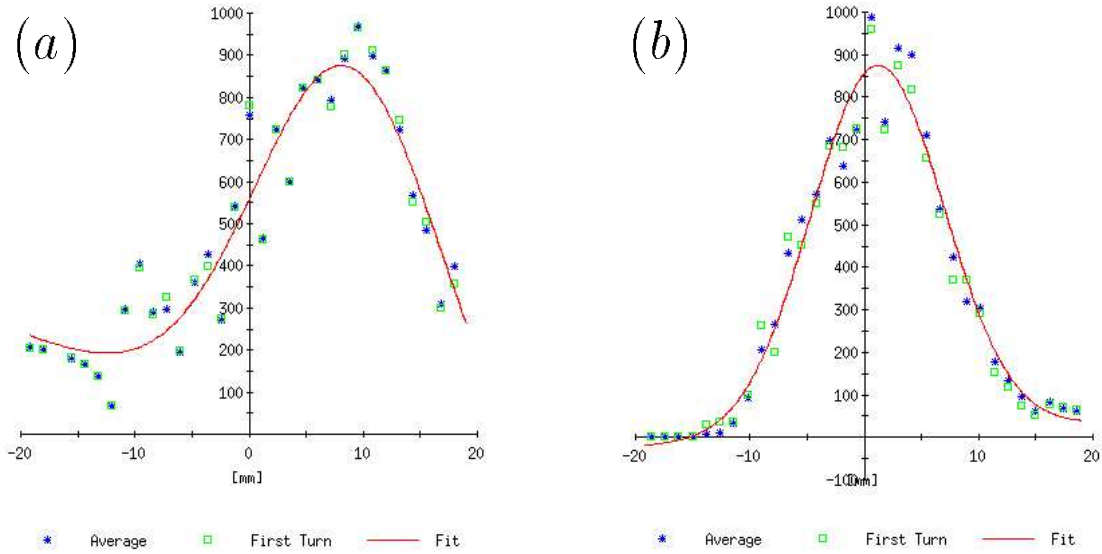


Figure 6: Horizontal ionization profile in part (a), vertical ionization profile in part (b). Shown are one turn, the average of 200 turns and a fit function. The fit is a superposition of a Gaussian function and a linearly sloped background function. Only even channels are depicted in the horizontal profile, only odd channels in the vertical profile.

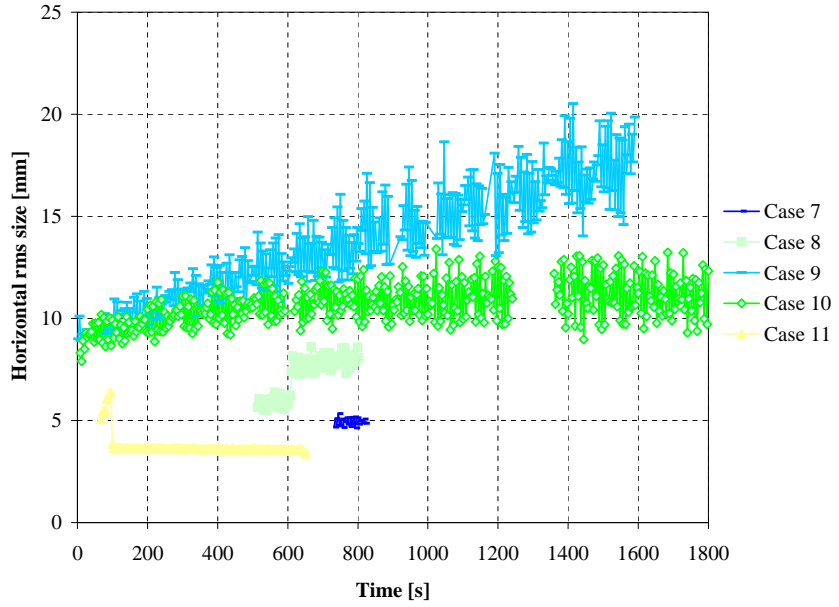


Figure 7: Horizontal beam size growth as observed with the ionization profile monitor. Shown are the standard deviations of fitted Gaussian distributions as a function of time. The data are likely to include a scaling error.

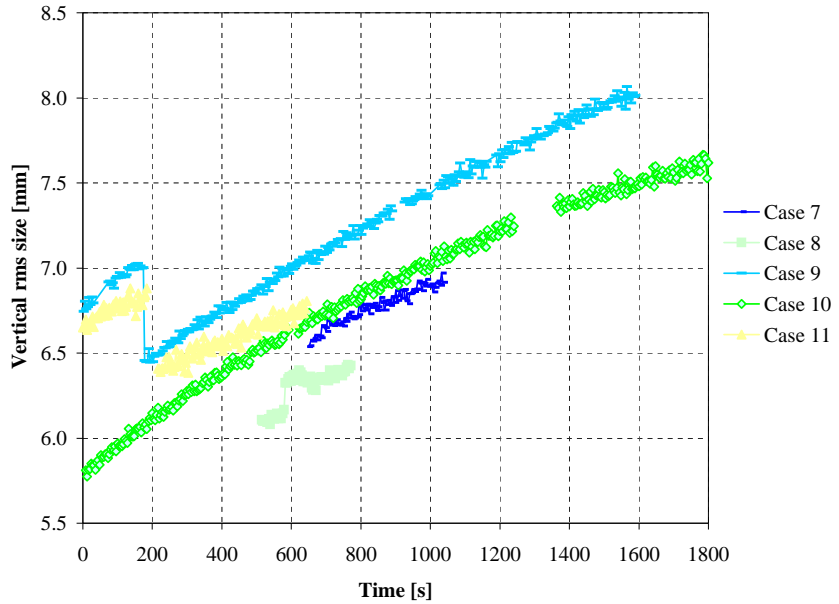


Figure 8: Vertical beam size growth as observed with the ionization profile monitor. Shown are the standard deviations of fitted Gaussian distributions as a function of time. During the first 200 s of case 8 and case 9 the beam size is overstated due to amplifier saturation.

2.4 Longitudinal Schottky Spectra

In Fig. 9 Schottky data are shown in the vicinity of the revolution line centered at $nf_0 = 2.7$ GHz. For single harmonic RF systems the power density in the longitudinal Schottky spectrum is well approximated by

$$P(f) = P_0 \sum_{m \neq 0} \int_0^{\hat{\tau}} d\tau \rho(\tau) J_m^2(2\pi n f_0 \tau) \delta(n f_0 + m f_s(\tau) - f), \quad (1)$$

where f is the measured frequency, nf_0 is the revolution harmonic closest to f , τ is the amplitude of the synchrotron oscillation in units of arrival time, and J_m is the Bessel function of the first kind. The density in amplitude is modeled as

$$\rho(\tau) \propto \tau(\hat{\tau}^2 - \tau^2), \quad \text{for } \tau < \hat{\tau}$$

and the synchrotron frequency variation with amplitude is taken to be

$$f_s(\tau) = f_s(0) \left(1 - \frac{(2\pi f_{rf} \tau)^2}{16} \right).$$

In actual measurements the intermediate frequency of the oscillator jitters, leading to a smearing of the measured spectrum. This washes out the fast oscillations in the Bessel functions so it is appropriate to take smoothed versions of these functions. A simple and effective approximation is

$$\langle J_m^2(x + \delta) \rangle_{\delta} \approx \min \left\{ \left(\frac{x^m}{2^m m!} \right)^2, \frac{1}{\pi x} \right\}, \quad (4)$$

where the angular brackets denote averaging δ over a range $|\delta| \lesssim 1$. Fig. 9 shows the result of optimizing $\hat{\tau}$, P_0 , $f_s(0)$ and the carrier offset frequency for a data set taken at injection energy. The optimized parameters $\hat{\tau} = 9 \pm 1$ ns and $f_s = 182.5 \pm 0.5$ Hz agreed well with independent estimates. While the measured Schottky spectra fit well to the described model, no change in the Schottky spectrum could be observed for the bunch length measurements reported here.

3 Analysis

In the measurements it was observed that the beam lifetime can vary significantly, and that the bunch length converges to a single value in most cases. Bunch length growth was observed for longitudinal well injected beams. In this section these observations are reviewed in more detail.

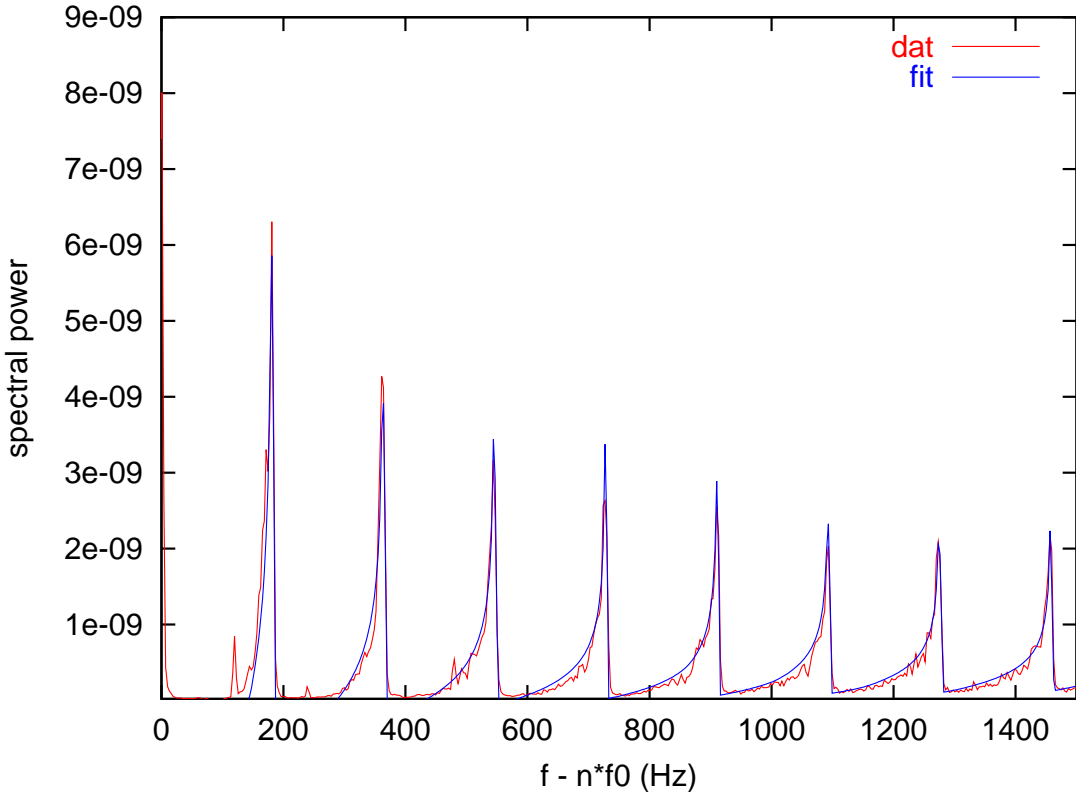


Figure 9: Schottky data in the vicinity of the revolution line centered at $n f_0 = 2.7$ GHz.

3.1 Beam Lifetime

With the data available, no mechanism could be identified that dominates the bunched beam lifetime. The lifetime appears not to be correlated with the longitudinal bunch area, the intensity, the longitudinal phase space density or the space charge tune shift. This observation is supported by the operational experience. Subsequent fills, only minutes apart, often have different beam lifetimes. In our measurements, cases 5 and 6 give such an example. Only 2 minutes apart, with no machine parameters deliberately changed, the lifetimes differ by an order of magnitude. One mechanism that may contribute to this is the known jitter in the AGS pulsed extraction elements. The jitter leads to different transverse beam sizes which may be correlated with lifetime. The transverse beam size measurements during this run, however, were not reliable enough to make a conclusion.

3.2 Asymptotic Bunch Length

In most measurements the bunch length converges to 5.0-5.5 ns. Initially long bunches shorten and initially short bunches grow. In addition, after a sufficiently long time all longitudinal profile can be well fitted to a Gaussian distribution. With an equilibrium

bunch length of 5.2 ns the bucket accommodates 3.4 standard deviations of a Gaussian distribution.

3.3 Intrabeam Scattering

Intrabeam scattering is the scattering of the particles in the beam from each other through the Coulomb forces that act between each pair of particles. It depends on the ion charge and mass like Z^4/A^2 and is usually larger for the heavier ions. Piwinski's original work [4] treated the case of constant beta functions and dispersion. This was later generalized by Bjorken and Mtingwa [5] and by Martini, Möhl, Piwinski and Sacherer [6] to include azimuthal variations of the lattice functions. Wei [7] simplified the computations for the case of pure FODO cells.

We only compute the longitudinal growth times since the intrabeam effect is most pronounced in the longitudinal plane. Furthermore, our transverse data are not fully reliable in both planes. The longitudinal growth time is defined as

$$\tau_s = \left(\frac{1}{\sigma_s} \frac{d\sigma_s}{dt} \right)^{-1} \quad (5)$$

where σ_s denotes the longitudinal rms bunch length and t the time. Similar definitions are used for the transverse dimensions.

We use two programs to compare measured longitudinal intrabeam scattering growth times with computations. Program 1 [8] is written by G. Parzen and is based on Ref. [6]. Program 2 [9] is written by J. Wei and is based on Ref. [7].

3.3.1 Simulations Program 1

In Ref. [6] it is assumed that the initial distribution of the particles in the transverse and longitudinal coordinates is Gaussian, and is described by $\epsilon_x, \epsilon_y, \sigma_p$, where ϵ_x, ϵ_y are rms transverse emittances and σ_p is the rms longitudinal momentum spread. The distribution is then assumed to remain Gaussian with time, while $\epsilon_x, \epsilon_y, \sigma_p$ change with time as a result of intrabeam scattering. One can then find expressions for the growth rates $d\epsilon_x/dt, d\epsilon_y/dt, d\sigma_p/dt$. The expressions for the growth rates contain a multiple integral which has to be evaluated numerically for each element of the lattice and averaged over the accelerator. This is done by the IBS.p program [8] using the lattice of the accelerator. The expressions for the growth rates can be integrated in time to find $\epsilon_x, \epsilon_y, \sigma_p$ at any later time. The results of the theory have been tested experimentally by Conte and Martini [10] using the AA ring at CERN, and by Evans and Gareyte [11] at the SPS.

3.3.2 Simulations Program 2

In the code it is assumed that the whole machine consists of FODO cells. The input consists of the FODO cell parameters, particle parameters like mass and charge state, beam parameters as transverse and longitudinal emittances and the bunched intensity.

The program calculates the longitudinal and transverse beam dimensions as a function of time along with the longitudinal and transverse growth times. In Ref. [7] the longitudinal growth rate (the inverse of the growth time) is computed as

$$\frac{1}{\sigma_s} \frac{d\sigma_s}{dt} = \frac{Z^4 N_b}{A^2} \frac{r_0^2 L_c (\beta c)}{8\pi(\beta\gamma)^4 \epsilon_x \epsilon_y \epsilon_s} F(\chi) n_b (1 - d^2) \quad (6)$$

where ϵ_x , ϵ_y and ϵ_s denote the unnormalized transverse and longitudinal [12] rms emittances. For bunched beams N_b is the number of particles per bunch and $n_b = 1$, for unbunched beams N_b is the total particle number and $n_b = 2$. L_c is a form factor which is approximately 20. If vertical dispersion can be neglected, one has

$$d = \frac{D_x \sigma_p}{(\sigma_x^2 + D_x^2 \sigma_p^2)^{1/2}}, \quad a = \frac{\beta_x d}{D_x \gamma}, \quad b = \frac{\beta_y \sigma_x}{\beta_x \sigma_y} a \quad \text{and} \quad \chi = \frac{a^2 + b^2}{2}. \quad (7)$$

The function $F(\chi)$ is defined by

$$F(\chi) = \frac{(1 + 2\chi)I(\chi) - 3}{1 - \chi} \quad \text{with} \quad I(\chi) = \begin{cases} \frac{1}{\sqrt{\chi(\chi - 1)}} \operatorname{arctanh} \sqrt{\frac{\chi - 1}{\chi}} & \chi \geq 1 \\ \frac{1}{\sqrt{\chi(1 - \chi)}} \operatorname{arctan} \sqrt{\frac{1 - \chi}{\chi}} & \chi < 1 \end{cases} \quad (8)$$

3.3.3 Results

Only five of the twelve measured cases show a longitudinally growing bunch. To measure the growth time in Eq. (5), the rms bunch length curves in Fig. 3 were fitted with a polynomial from which the growth times could be determined analytically. The fitted curves are shown in Fig. 10 and the obtained growth times are shown in Tab. 4. Typically a polynomial of fifth order was used for the fit. An estimate for the error of the measured growth rates can be obtained by fitting polynomials of different orders to the experimental data. When polynomials of order two to five are used, the obtained growth rates vary by up to 35% around the average value, while the R^2 of the fit changes only little. Note that growth rates and growth times are derivatives of a measured function and therefore sensitive to small local changes in the measured function.

For all cases for which a bunch length growth was observed, the bunch length growth was also computed with both programs using the initial bunch length, transverse sizes, and intensity. For both the horizontal and vertical emittance, the average measured vertical emittance was used in the computations. The machine was fully coupled in all cases (compare Tab. 3) and the vertical emittance measurement much more reliable than the horizontal one. The growth time was computed with the beam parameters at the beginning and end of a measurement. The computed longitudinal growth times are shown in Tab. 4.

In all but one instance (case 11, final), the computed growth time is larger than the measured growth time. Computed growth times exceed measured growth times by up to

Table 4: Comparison of measured and computed longitudinal growth times τ_s from intrabeam scattering.

Case	measured $\tau_{s,m}$ [min]	initial			measured $\tau_{s,m}$ [min]	final		
		$\tau_{s,c}$	$\frac{\tau_{s,c}}{\tau_{s,m}} - 1$	$\tau_{s,c}$		$\tau_{s,c}$	$\frac{\tau_{s,c}}{\tau_{s,m}} - 1$	$\tau_{s,c}$
1	53	114	115	120	125	179	199	11
2	183	335	94	366	100	361	426	18
3	208	316	52	357	73	273	405	48
11	110	127	15	136	23	464	290	-37
12	165	167	1	171	4	361	324	-10
							370	3

125%, with an average of 50%. This constitutes a satisfactory agreement given the 35% error in the growth time measurement.

In Fig. 10 the bunch length development of the five simulated cases is shown. The measured and computed bunch lengths are depicted. Except for the case starting with the smallest bunch length (case 1) there is a relatively good agreement. Case 1 is the case with the largest growth rate and a source other than intrabeam scattering may have contributed significantly to the bunch length increase. Note that in the simulations the particle loss observed in the measurements (see Fig. 2) is disregarded, which artificially increases the computed bunch length growth rate by up to 30% at the end of the computation period (see Tab. 1 and Eq. 6). This error has the same magnitude as the measurement error for the growth rates.

The results of simulation program 1 and simulation program 2 show one significant difference in the transverse growth rate. Program 1 predicts a slowly increasing beam size in both transverse planes while program 2 predicts a beam that is shrinking in both transverse dimensions. A transversely shrinking beam is expected if the bunch behaves like a gas in which energy is transferred from the hotter transverse dimensions to the cooler longitudinal dimension. However, no transverse shrinkage was observed, the beam grew transversely.

4 Summary

Emittance growth of bunched gold beams were observed at injection. Observed growth rates vary significantly from measurement to measurement. So far, no dominating transverse growth mechanism could be identified. The most significant mechanism for longitudinal bunched beam growth is intrabeam scattering. Comparisons with two computer codes give an agreement between measured and computed growth times within a factor of two or better.

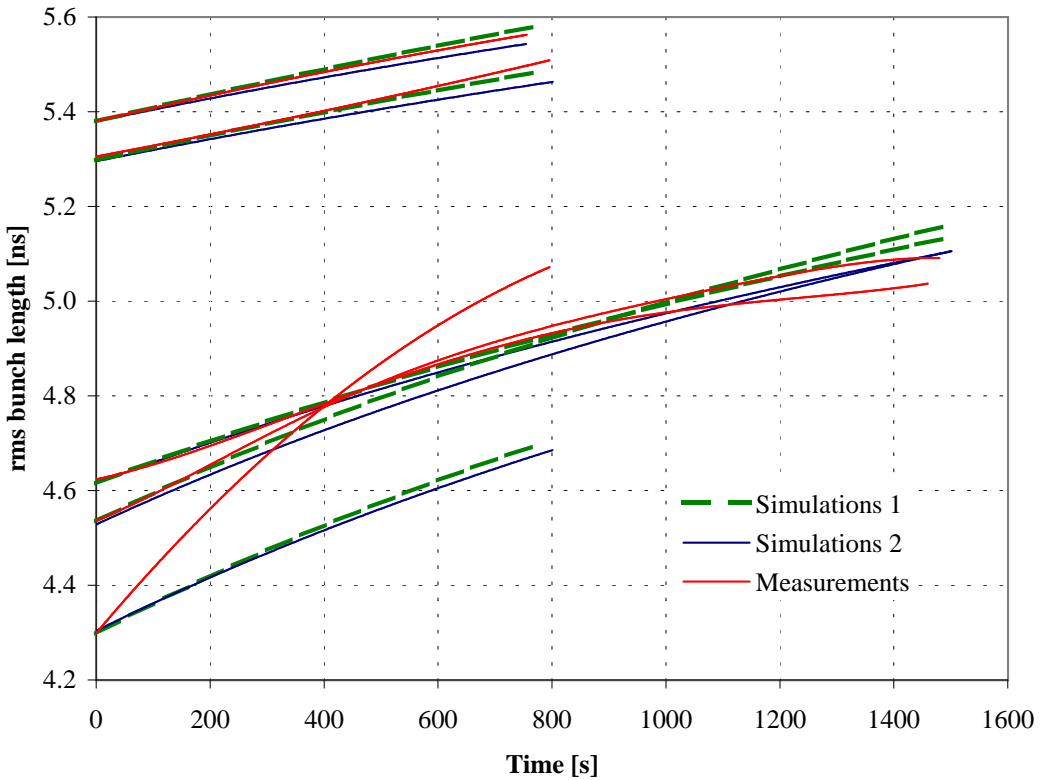


Figure 10: Comparison between measured and computed bunch length growth.

5 Acknowledgments

The authors are thankful to the operations, instrumentation, radio frequency, control and accelerator physics teams that supported the data acquisition, storage, processing and analysis in many ways. In addition, we are thankful to J. Wei and H. Hahn for discussions.

References

- [1] J. Wei, “Intra Beam Scattering in RHIC”, BNL RHIC/AP/63 (1995).
- [2] W. Fischer, W.W. MacKay, S. Peggs and J. Wei, “Emittance Growth in RHIC During Injection”, proceedings of the LHC96 Workshop on High Brightness Beams for Large Hadron Colliders, Part. Acc. Vol. 58, pp. 181-191 (1997) and BNL RHIC/AP/112 (1996).
- [3] W. Fischer, M. Giovannozzi and F. Schmidt, “Dynamic Aperture Experiment at a Synchrotron”, Phys. Rev. E, Vol. 55, Number 3, p 3507 (1997).

- [4] A.Piwinski, proceedings HEAC 74, Stanford, pp. 405 (1974).
- [5] J.D. Bjorken and S.K. Mtingwa, “Intrabeam Scattering”, Part. Accel. Vol. 13, pp. 115-143 (1983).
- [6] M. Martini, “Intrabeam Scattering in the ACOL-AA Machines”, CERN PS/84-9 (AA) (1984).
- [7] J. Wei, “Evolution of Hadron Beams under Intrabeam Scattering”, proceedings of the 1993 Particle Accelerator Conference, Washington, D.C. pp. 3561 (1993).
- [8] G. Parzen, “Intrabeam Scattering at High Energies”, Nuc. Inst. Meth. A245, pp. 231-240 (1986).
- [9] Computer program by J. Wei, private communication (1993).
- [10] M. Conte and M. Martini, “Intrabeam Scattering in the CERN Anitproton Accumulator”, Part. Accel. Vol. 17, pp. 1-10 (1985).
- [11] L.R. Evans and J. Gareyte, PAC 85 (1985).
- [12] S. Peggs and J. Wei, “Longitudinal Phase Space Parameters”, BNL RHIC/AP/106 (1996).